



Maastricht University

MSP RESEARCH PROJECT 310

Cosmic Watch: Reloaded - Mapping the Asymmetry of Local Muon Flux

MAASTRICHT SCIENCE PROGRAMME

2023-2024

Student Leaders & Authors:

Emre Berna, Mathias Perazo, Nils Thiessen

Authors:

Pedro Afonso, Laura Brijan, Karsten Dekkers, Tom Kores Lesjak, Miguel Miralda Porrero,
Grzegorz Ratajski, Enrique Sanchez, Indra Vezbergaite

Project Coordinator:

Chad Ellington

2nd July 2024



Contents

1	Introduction	3
1.1	Motivation	3
1.2	Source of Cosmic Rays and Muon Production	3
1.3	Functionality of the Cosmic Watch Muon Detector	5
1.3.1	Scintillator and Photomultiplier	5
1.3.2	Coincidence Measurements	6
1.4	Focused Coverage Area	6
1.5	Effect of Geomagnetic Field on Cosmic Rays	7
1.5.1	East-West Asymmetry	8
1.5.2	Variance of East-West Asymmetry	8
1.6	Hypothesis	9
2	Methodology	10
2.1	Components	10
2.2	Construction	10
2.3	Calibration	11
2.4	Experimental Setup	13
3	Results & Analysis	15
3.1	Results	15
3.1.1	Calibration Ratios	15
3.1.2	Directional Rates	15
3.2	Analysis	16
3.2.1	Probable Error on Counts	16
3.2.2	Flux and Asymmetry	17
3.3	Unused Data	19
4	Discussion	20
4.1	Limitations & Improvements	20
4.1.1	Angular Alignment of the Setup	20
4.1.2	Detector Holder Construction Inaccuracies	21
4.1.3	Lacking SD Card Readers in Master Devices	21



Contents

4.1.4	Cosmic Watch Event Silence and Sensitivities	21
4.2	A Subtle Phenomenon	22
4.3	Unclear Case for Calibration Method	23
4.4	Comparison to Literature	24
5	Conclusion	25
6	Appendix	28
6.1	Referenced Figures	28
6.2	Contributions	29
6.2.1	Experiment	29
6.2.2	Paper	30



1 Introduction

1.1 Motivation

The existence of natural radiation on Earth has long been established, causing air in electroscope chambers to randomly ionize [1]. Early theories proposed that this radioactivity was a result of how Earth's crust was composed, which prompted several research groups [2] to conduct experiments at varying altitudes to determine the absorption of γ -radiation in air. These balloon ascents led to the discovery of a different source of radiation that increased with altitude, which was later recognized as a direct consequence of cosmic rays.

Further related studies expanded knowledge about cosmic rays, their origin and propagation through the universe, as well as effects of the geomagnetic field. Furthermore, research into particle physics was propelled as a consequence, leading to the discovery of muons by Carl D. Anderson and Seth Neddermeyer in 1936 [3].

Coincidentally, the radiation found during the balloon ascents was mostly comprised of muons, from which it has become apparent that these leptons make up most of the cosmic radiation found at sea level [4].

Over the years, detectors have developed from Geiger counters [5] to large-scale construction like the Super-Kamiokande. In addition to that, tracking the muon flux caused by cosmic rays has become accessible and compact through a portable device created by the CosmicWatch group [6].

Previous project groups worked on constructing and setting up several Watches. As a result, four of the detectors were ready at the beginning of the current experiment, and two more were added. Putting the detectors to full use, they can be tested and implemented to assess phenomena related to cosmic rays such as the East-West asymmetry.

1.2 Source of Cosmic Rays and Muon Production

Cosmic rays are relativistic particles originating from outer space astronomical events, such as supernovae, and from celestial bodies like the Sun, notably during solar flares [7]. Low-energy charged particles most likely stem from within the Milky Way, accelerated by fast-moving magnetic fields in a process called Fermi shock acceleration. Conversely, the trajectory and high energy of some cosmic rays suggests that their source should lie beyond the bounds of our galaxy [8].

A majority of the cosmic ray mass flow density on Earth consists of 74% ionized hydrogen, 18% helium nuclei, and the rest is contributed by heavier elements [6]. Some of these primary particles are bound to hit Earth due to their trajectory, during which they interact with Earth's atmosphere and magnetic fields. These interactions can cause the rays to be deflected (change in trajectory) or blocked. However, some cosmic rays still make it past these boundaries. In that case, they can be split by Earth's atmosphere, causing a shower of secondary particles which can be observed by equipment such as the Cosmic Watch muon detector used in this project. Furthermore, the source of these particles cannot be accurately determined. Since they are influenced by magnetic fields and other obstructions, the initial and final trajectories differ. Yet, measuring the energy of these particles could help predict which forces acted on them and, therefore, identify their sources [9].

As the primary cosmic rays bombard Earth's exosphere, they interact with high energy particles present in the atmosphere. This can either break the target particle, the primary particle or both due to the strong force acting upon them. These collisions produce mesons, most commonly $\pi^{+,-,0}$ (pions) and $K^{+,-,0}$ (kaons). The neutral mesons decay too quickly to interact with other particles. However, charged mesons have a greater lifetime and allow further interactions with particles deeper in the atmosphere, producing more mesons. These can then decay into muons causing a scattering effect. This decay tree is shown in Figure 1.

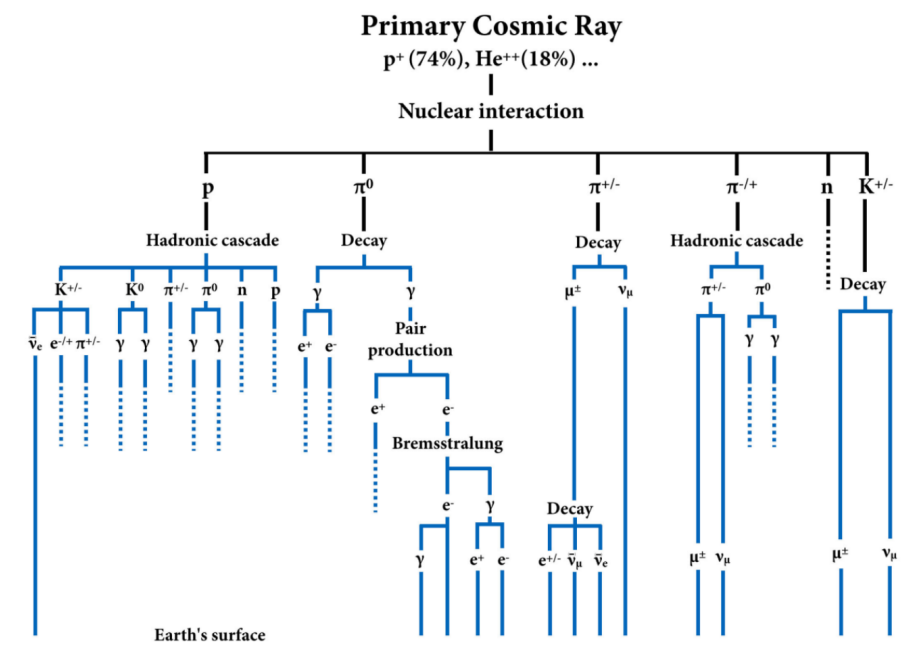


Figure 1: Decay of cosmic rays[6]

As neutral mesons have a short lifetime, the muons produced during their decay do not have sufficient energy to reach Earth before decaying and are therefore ignored. The most relevant reactions are thus the following:



Kaons can decay into pions. This reaction is therefore also considered:



From these decays the muons will have sufficient energy to travel to Earth's surface and can be detected by the Cosmic Watch [6].

1.3 Functionality of the Cosmic Watch Muon Detector

1.3.1 Scintillator and Photomultiplier

The Cosmic Watch detects muons using two main components: the scintillator and the photomultiplier, where the scintillator absorbs muon hit energy and the photomultiplier thereafter converts it into a measurable signal. A scintillator takes in energy through electrostatic interactions, and re-emits the same amplitude of energy in the form of photons. When radiation comes in contact with the scintillator, its energy will excite the electrons, raising their energy levels. After de-excitation, a photon is emitted [10]. As will be discussed in Section 2.2, an organic plastic scintillator is most relevant to the context of this experiment. This plastic scintillator consists of 3 layers: first comes a transparent base which must be in the visible light spectrum. It has the purpose of holding the other fluorescent layers together and allows the propagation of light through it. Next comes the primary fluorescent agent. When a muon or other particle interacts with this layer, the electrons within get excited. The de-excitation of the material then leads to an emission of ultra-violet light. This light travels to the secondary fluorescent layer, where it is absorbed and light in the visible spectrum is emitted before travelling throughout the rest of the scintillator [6].

Photomultipliers are used to amplify the signal generated from particles interacting with the scintillator, resulting in a measurable signal which lasts around 1 μ s [11]. For this detector, silicon photomultipliers (SiPMs) are used, since they have a few advantages when compared

to other photomultipliers. For example, SiPMs can operate at relatively low voltages, they are not sensitive to changes in magnetic fields, and have a relatively small build. An Arduino that searches for a pulse every $6\ \mu\text{s}$ is connected to this system. This means that it is possible for the signal to be missed by the Arduino. Ergo, a peak detection circuit has to be implemented to amplify and stretch the duration of the signal to a greater range, such that the Arduino can detect all the signals that were initially emitted.

1.3.2 Coincidence Measurements

In this study, only coincidence measurements were considered, in which a muon hit event is only recorded if it is registered on multiple devices at the same time. This measurement mode includes two devices connected by a coincidence cable, which has a signal delay of $\sim 30\ \mu\text{s}$. Two detectors set up in coincidence mode in such a manner make up a master-slave system. When the master registers an event, it sends a signal to the slave system which takes $\sim 30\ \mu\text{s}$ to decide whether to save or discard the event. If the slave system also registers an event at the same time as the master, the event is saved as a muon hit. This is a valid assumption based on the properties of muons. A muon can only interact via the electromagnetic and weak force, which means it has a high penetrative property. Hadrons, for example, do not have such a property, as they interact through the strong force and will lose more energy when passing through material. In addition to that, muons are heavier than electrons, meaning that they carry more momentum which allows them to resist changes in trajectory. Muons also have longer decays compared to other particles that may register on these detectors. Therefore, they will not decay or exceed the energy threshold needed to penetrate both detectors.

1.4 Focused Coverage Area

In order for a detector pair to cover a specific area of sky, the detectors must be placed at a certain distance from each other. This distance can be inferred using Figure 2.

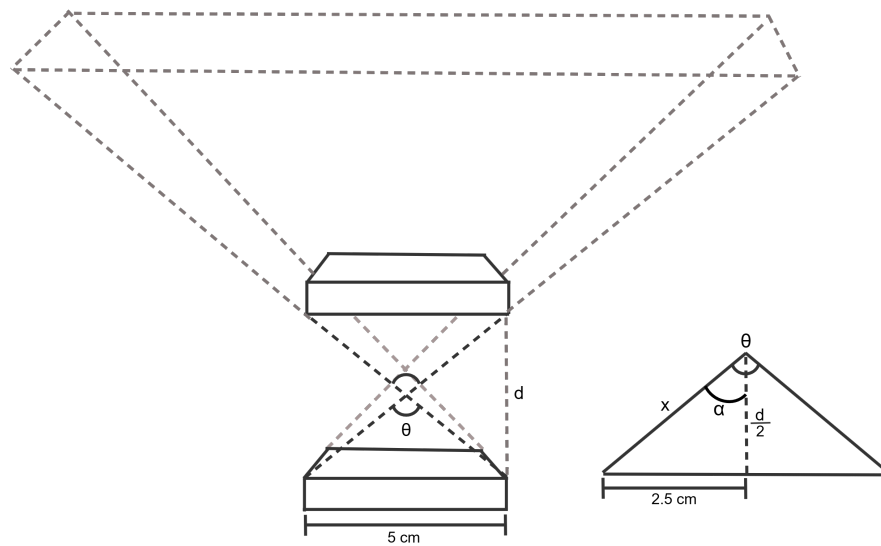


Figure 2: Cosmic Watch Focused Coverage Area

The distance between the detectors for them to cover an angle $\vartheta = \alpha \cdot 2$ is now given by the following formula:

$$d = \frac{5}{\tan(\alpha)} \quad (3)$$

where d is the distance between the scintillators (in cm). It is also important to set the detectors up in such way that there is no considerable obstruction between them and space, to ensure the number of muon detections is not reduced by them.

1.5 Effect of Geomagnetic Field on Cosmic Rays

The differences in the amount and type of muon flux one measures on Earth's surface is primarily decided during passage of cosmic rays through Earth's magnetosphere.

The magnetic field impacts the path cosmic rays take upon approaching Earth, which is correlated to the energy of the particle. Generally, lower momentum results in a higher degree of deflection along the trajectory of motion. Low-energy cosmic rays are therefore either shielded off before entering the atmosphere, or trapped inside the inner radiation belt (one of the van Allen belts) [12]. This magnetic field, a domain of Earth's magnetosphere, mainly confines protons oscillating between two locations in each hemisphere, mirrored along the equator as seen in Figure 3.

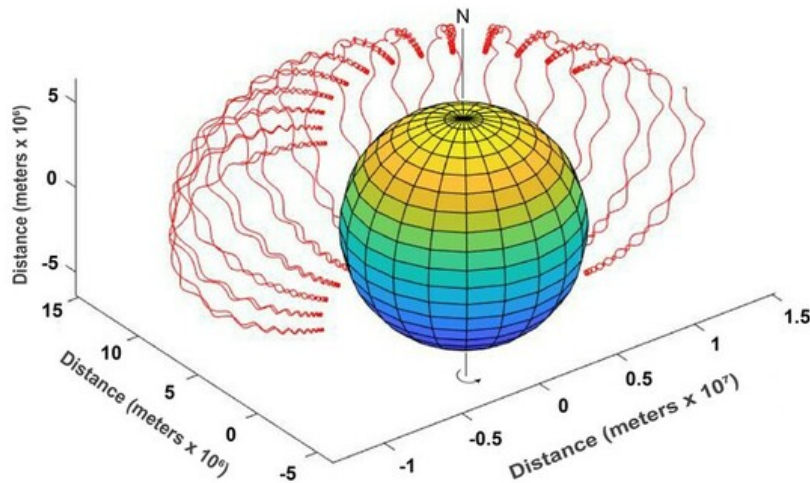


Figure 3: Trajectory of magnetically trapped low energy protons, as found at the inner van Allen belt. The particles will oscillate between two mirror points under the influence of the geomagnetic field. Simulation conducted by Vikarn Rajora and Federico Nova [12].

While high-energy particles only deviate slightly from their initial trajectory, interactions during their passage of the atmosphere often create neutrons. These later decay to protons, which frequently still takes place inside the belt [13, p.17].

1.5.1 East-West Asymmetry

A more subtle effect of the magnetic field could be found in the deflection of cosmic ray particles towards the East, which originally led to the conclusion that they must be largely positively charged [14]. The interaction between the field lines and the particle's movement occurs according to the Lorentz Force. Similarly, positive particles already possessing a westwards component are curved away from Earth, while an eastward component leads to a trajectory towards Earth. Both of these deflections lead to a higher cosmic ray intensity from the West [12]. This East-West asymmetry causes a larger amount of primary cosmic rays to arrive from the West compared to the East, which also translates to the muons measured at surface level. The extent of this asymmetry depends on several factors.

1.5.2 Variance of East-West Asymmetry

One of such factors is the latitude effect. Near the geomagnetic equator, where incoming particles on a course towards Earth are at the highest angle relative to the magnetic field, their paths are bent more strongly. Cosmic rays will thus have a high tendency to proceed

eastwards. As a result, the East-West asymmetry is most pronounced near the geomagnetic equator, decreasing towards the geomagnetic poles. Under similar conditions, the East-West asymmetry coefficient A was found to be approximately 0.055 at geomagnetic latitude 41°N and 0.21 at 9°N [15].

One aspect to consider is that the asymmetry is largely caused by low-energy cosmic rays. As the muons carry on their parent's momentum and pass through atmosphere, they lose energy relative to their path length. Low-energy muons are therefore more likely to decay, which becomes particularly apparent when taking measurements at large zenith angles. Additionally, when comparing the flux at same large angles East and West of the zenith, the rates should stay similar. As such, the coefficient of asymmetry reaches a maximum at approximately 43° [5].

Even then, the magnitude of this effect varies in time. The deviation can be associated to changes in the geomagnetic intensity, thereby alternating the lower limit of the energy necessary for cosmic rays hitting Earth [16]. Furthermore, high solar activity causes an increased deceleration of cosmic rays, resulting in smaller relative amounts of low-energy particles. Considering this, the East-West asymmetry should become lowest at solar maximum [17, p.151].

1.6 Hypothesis

Considering the effects of the Earth's magnetosphere on incident cosmic ray particles, the dominance of Western muon flux upon the surface should be found when two Slave-Master pairs of Cosmic Watch muon detectors are set to measure flux incoming from Eastern and Western portions of the celestial sphere. If overall muon fluctuations across different measurements are accounted for with a third calibration pair, this effect can be shown explicitly and provide an argument for the overall charge of the original cosmic ray particles.

2 Methodology

2.1 Components

Component Name	Amount	Component Name	Amount
22pF capacitor	4	10uF capacitor	6
0 Ohm resistor	10	Ferrite bead	4
0.1uF capacitor	8	47uH inductor	2
249 Ohm resistor	4	Schottky diode	4
1k resistor	8	4 pin header for OLED	2
10k resistor	4	Temperature sensor	2
24.9k resistor	4	Reset button	2
100k resistor	6	Standoff threaded screws 0.80	8
226k resistor	4	6-pin connector	2
10pF capacitor	4	Non-inverting Buffer	2
0.47uF capacitor	4	Standoff for SiPM PCB	4
20nF capacitor	12	5mm LED	2
49.9 Ohm resistor	8	SiMP	2
1uF capacitor	6	Main PCB + SiPM PCB	2
10nF capacitor	8	Rubber feet	8
3.3V regulator	2	Aluminum case	2
LT-3461 DC-DC Booster	2	Circuit housing	2
LT-1807 OP-Amp	2	Optical gel	2mL
Arduino Nano	2	Coincidence cable	2
OLED screen	2	BCN cable	2
6-pin header	2	Electrical tape	2m
3.5mm coincidence jack	2	Aluminum foil	1
5mm LED holder	2		

Table 1: List of Components for Building 2 Cosmic Watches without SD Card PCB

2.2 Construction

The process of building the detectors followed the Cosmic Watch Project [18], but was adapted to specific requirements of this experiment. All components listed above were needed for the constructing of the muon detectors, and they were soldered according to the Cosmic Watch Circuit Diagram 11, which can be found in the Appendix Section. The circuit is divided into three circuit boards: the main, SiPM and SD Card PCBs.

The first step to populating the main PCBs was to solder the small components, including inductors, capacitors, diodes and resistors on it. The next step was to solder the integrated circuits, namely the OP-AMPS and DC/DC converters, on the PCBs. After this the audio

2 Methodology

connection jacks, temperature sensors, tactile switches, LED lights, and the Arduino nanos were attached to the main PCBs. Then an oscilloscope was used to check for the presence and characteristics of the signal on various locations on both of the main PCBs. All the soldering was performed using a soldering iron and a lead-free solder.

Next, similar to the main PCBs, the first step was to solder the small components onto the SiPM PCBs. Afterwards, a hot air gun was used to polish the organic plastic scintillator until it turned transparent. The scintillator was subsequently wrapped in aluminum foil, in order to maximize the internal reflection of light and to avoid interference due to infrared radiation. It was then secured with electrical tape, leaving a 2x2 cm opening for the photomultiplier. Optical gel was applied to the photomultiplier, and it was placed on the opening. Finally, this scintillator and SiPM PCB assembly was tightly covered with black electric tape, making it secure against any external light penetration inside the detector. Following the assembly of the PCBs, the SiPM PCBs were connected to main PCBs and placed in their housings.

2.3 Calibration

The Cosmic Watches were initially powered by connecting them to a laptop. The first step in the calibration process was to set all six cosmic watches, two that were just built and four that were built during previous projects, to master mode and register their sensitivities based on the amount of triggers they register in a certain amount of time. In order to keep track of the muon detectors, they were given names and numbers. In the next step, different combinations of cosmic watches were tested based on these sensitivities, in order to find three pairs of detectors with similar overall counts. Within the two detecting pairs that were chosen, detectors Billy and Bob were set to slave mode.

During observations made before the project started, it was noticed that the muon flux was inconsistent over a period of time, as shown in Figure 4:

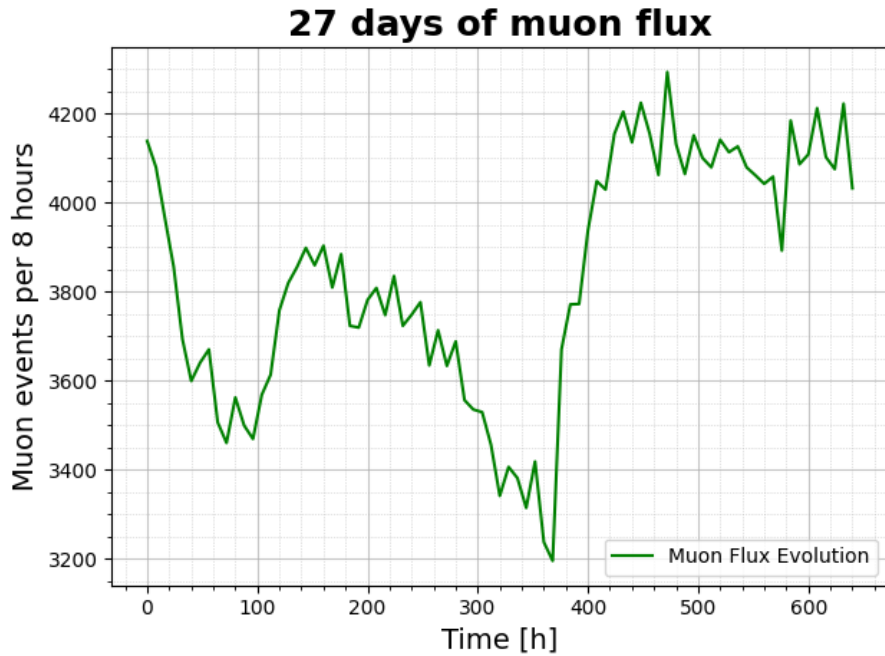


Figure 4: 27 day evolution of muon detections every 8 hours. It can be seen that rates fluctuate significantly over the course of days. Measurements were taken in a residential building at the bottom floor.

Short term fluctuations most likely arise randomly, while long term changes (across days or weeks) are caused by certain astronomical events such as solar flares [7].

This could have become an issue when searching for an East-West asymmetry, as the measurements would likely occur under distinct conditions. To fix it, a pair of master-slave detectors were assigned to act as calibration devices. These would constantly observe the whole sky, thereby recording variations in the overall muon flux.

For all detector sets, the muon events in a certain time interval were counted, and the detection rate was established using $R = \frac{\text{Events}}{\text{Time}}$. The idea of the calibration watch was to observe how this rate deviated from an earlier specified reference value, recorded as the ratio $\frac{R_{\text{ref}}}{R[X]}$. The actual data, as gathered from the other detectors, was then multiplied with the ratio of the corresponding time interval. Here, the calibrated data should show how every measurement would look like under the same conditions of muon flux, as the overall time variation of events is thereby taken into account.

The reference value was chosen to be the average muon rate, so that a clear comparison could be made to other experiments. However, it is worth noting that for the calculations of the asymmetry, which observes the percentage deviation of the calibrated values from one another, the choice of reference value is irrelevant.

2 Methodology

The calibrated rate Z'_n can thus be calculated by:

$$Z'_n = \frac{\bar{R}}{R_n} \cdot Z_n \quad (4)$$

Here, R corresponds to the detection rate of the calibration Watch, while Z represents the rate of the actual data. \bar{R} portrays the mean rate of the calibration Watch, chosen as the reference value.

2.4 Experimental Setup

In order to accurately position and orient the Cosmic Watches, two wooden support structures were built, one for each measurement pair. A single structure consisted of two wooden beams and a metal rail with two slidable supports. To construct this structure, each wooden beam was first cut at a $45\pm0.4^\circ$ angle from one edge and were connected to each other using flat metal plates, resulting in a structure similar to an "L" shape. A metal rail was screwed onto the longer wooden beam, fixing it in place. Two support seats were attached onto this rail, one for each Cosmic Watch, which allowed the incidence angle covered by the watches to be changed by adjusting the distance between them. These steps were repeated once again, ultimately yielding two of these structures. In order to make it possible to do two accurate measurements at the same time, the structures were secured to the bottom of a plastic box using right-angle metal brackets. Inside the plastic box, the two structures were oriented 180° relative to each other such that they were directly facing in opposite directions. The box was then placed inside a car with a glass roof and covered with a heat blanket, in order to avoid infrared radiation from interfering with the experiment.



Figure 5: Top view of muon detectors setup.



Figure 6: Side view of muon detectors setup.

2 Methodology

The two wooden structures were pointed in opposite directions and the muon detectors were placed on the rail, at a 45° angle with the horizon, as shown ideal in Section 1.5.2 . The Cosmic Watches were separated by 18.30 ± 0.05 cm, in order to cover 30° of the sky at a time. This set up was rotated by 30° two times, measuring for seven hours in each position and covering a total 90° area of sky in both the East and West directions. The rotation process was performed by rotating the car 15° , and rotating the box by 15° inside the car, in order to ensure both detector pairs would be aimed at a window. This was done so that the muon detectors were exposed to the same shielding materials for all measurements. In order to rotate the car and box by a set amount of degrees, a compass was used to align the car with the East-West direction, and then again for the smaller rotations of 15° . However, due to the inherent magnetic field of the car interfering with the compass, the compass could only be used outside of the car.

Simultaneously, the two remaining muon detectors were placed flat on the ground directly on top of each other, in order to detect as many muons as possible. This was to measure the baseline muon flux affecting the earth during the times of measurement, to be able to compare measurements made at different times.

Observation took place inside a Honda Jazz in the UM Sports parking lot from Friday the 21st of June until Wednesday the 26th of June.

3 Results & Analysis

3.1 Results

3.1.1 Calibration Ratios

Figure 7 illustrates the evolution of muon flux throughout the days as measured by the set of calibration watches. Due to weather conditions (further explained in Section 4.1.4), data was predominantly gathered at night.

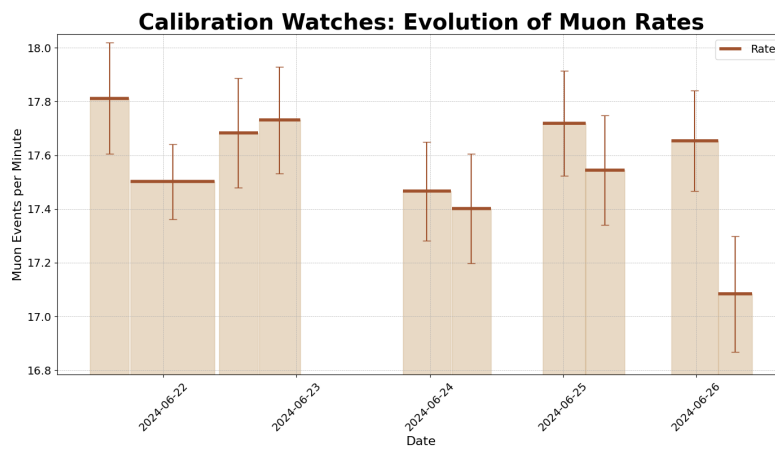


Figure 7: Calibration Watch: Plot showing the evolution of muon rates throughout the course of the experiments. The length of the horizontal bars represents the duration of each measurement.

The mean of the muon rates was established to be roughly $17.539 \frac{\text{det}}{\text{min}}$, according to Figure 7. Implementing this as a reference value, one could then determine the calibration ratios for each time interval.

3.1.2 Directional Rates

After the data was collected at different angles with respect to North, the following detection rates were calculated:

Before Calibration

Azimuth Angle [°] $\pm 13^\circ$	Rate Billy [det/min]	Rate Bob [det/min]
60	0.494185746	0.440392206
90	0.489994182	0.479356122
120	0.489190026	0.437574318
240	0.486743376	0.461298690
270	0.558028620	0.457501962
300	0.555375270	0.465961572

Table 2: Before calibration: Detection rate values of detectors Billy and Bob pointing in different azimuthal directions. Azimuth Angle describes the angle at the center of the 30° range covered by the Watches.

From the previously established ratios, the data was calibrated as explained in Section 2.3:

After Calibration

Azimuth Angle [°] $\pm 13^\circ$	Rate Billy [det/min]	Rate Bob [det/min]
60	0.507373980	0.44349165
90	0.486821190	0.474323112
120	0.493621986	0.435243042
240	0.490169040	0.473609274
270	0.552169590	0.454539378
300	0.552416382	0.470183088

Table 3: After calibration: Detection rate values of detectors Billy and Bob pointing in different azimuthal directions. Azimuth Angle describes the angle at the center of the 30° range covered by the Watches.

It is notable that due to the minute fluctuations observed by the calibration Watches, there has not been a big change in the rates between Tables 2 and 3.

3.2 Analysis

3.2.1 Probable Error on Counts

The estimation of error in a single, instantiated measurement of muon counts from a certain direction relies on Poisson (or Gaussian) statistical approximations. The fundamental principle to rely on such concepts is that the repetition of a particular muon flux measurement may

3 Results & Analysis

show varied results which follow a Poisson distribution with a characteristic mean flux. It is conventional to take the error of a measurement that lies within this distribution to be one standard deviation in magnitude. To derive the implicit standard deviation of the sample distribution that the measurement was taken from, its mean must be approximated as the measured value itself, meaning $\bar{x} = x$, where x is the measured value belonging to the implicit distribution. Given that $\sigma^2 \cong \bar{x}$, the probable error of any measured muon count can be taken as $\sigma \cong \sqrt{\bar{x}}$ [19].

3.2.2 Flux and Asymmetry

Figures 8 and 9 show the muon events per minute, as measured at each angle. The measurements for each angle were performed once with both detector pairs in order to improve the accuracy of the experiment.

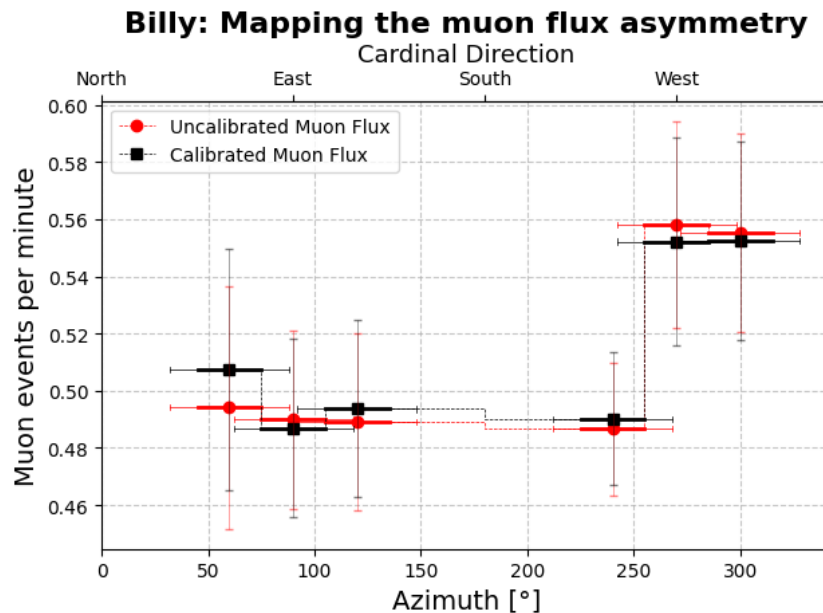


Figure 8: Detector Billy: Plot of muon flux at different ranges of azimuth angles, for both the calibrated and original dataset. The horizontal error bars represent the inaccuracy of the direction, while the vertical ones demonstrate the statistical error.

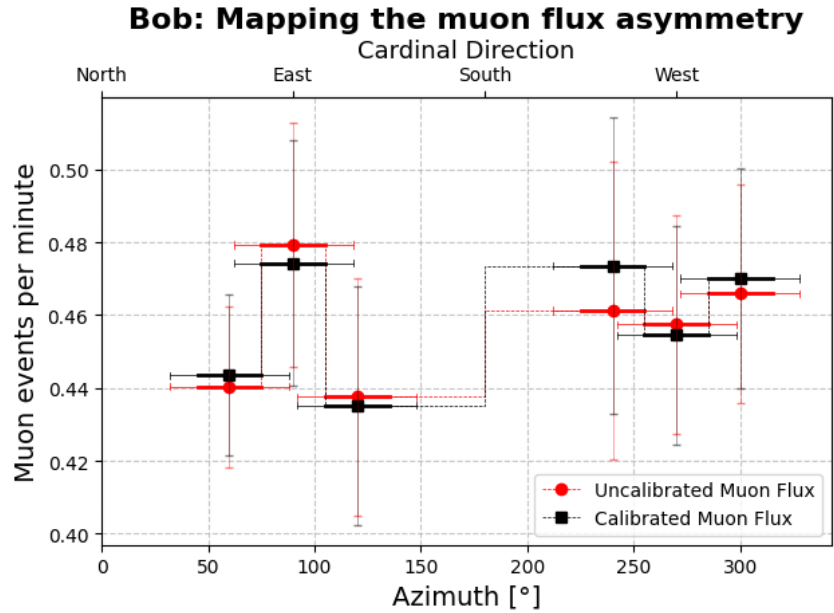


Figure 9: Detector Bob: Plot of muon flux at different ranges of azimuth angles, for both the calibrated and original dataset. The horizontal error bars represent the inaccuracy of the direction, while the vertical ones demonstrate the statistical error.

In Figures 8 and 9, the muon detection rate at each of the six angles that were measured with both pairs of detectors is shown. Both the calibrated and uncalibrated datasets are displayed on the plots, as well as error bars that show the uncertainty in the angle that was measured each time. In Figure 8 the detection rate from the West is higher than the one from the East, which is consistent with the East-West asymmetry that has been studied before [15]. Figure 9 shows that there were more detections from the East than from the West, which is the opposite of what was expected and what was measured by Billy.

The coefficient of East-West asymmetry is commonly calculated using Equation 5 [5]:

$$\alpha = 2 \cdot \frac{I_w - I_e}{I_w + I_e} \quad (5)$$

Wherein α is the asymmetry coefficient, and I_w , I_e the Western and Eastern flux rates in detections per minute. Utilizing this equation, the values for the asymmetry were:

Asymmetry (α) [unitless]	
Billy: Uncalibrated	0.1298338888623
Billy: Calibrated	0.1257920691077
Bob: Uncalibrated	-0.0466541525835
Bob: Calibrated	-0.0425977670818

Table 4: Asymmetry values for Billy and Bob before and after calibration

From table 4 and Figures 8 and 9, it can be inferred that the Cosmic Watches had different sensitivities. A positive value of α means that there were more muon detections coming from the West than from the East. Billy detected an asymmetry of around 0.13 and Bob detected one around -0.04.

3.3 Unused Data

Some of the measurements were disregarded due to various reasons, such as interference from the surroundings and temperature. The measurements made on the 22nd of June were not used in the calculations of the asymmetry, due to procedural error. Half of the measurements done on the 23rd of June were also disregarded due to the detectors overheating during the course of the experiment. It was also necessary to disregard half of the measurements made on the 24th and 25th of June because one of the detectors turned off at some point during the measuring, which is further explained in Section 4.1.4.



4 Discussion

4.1 Limitations & Improvements

4.1.1 Angular Alignment of the Setup

As explained in Section 2.4 the angular alignment of the detector relied mostly on quantitative methods. One source of uncertainty was the angular alignment of the car relative to the compass used. Considering that the measurements were performed in a parking lot with many cars which were observed to produce significant magnetic fields as seen on the compass, the uncertainty stemming from the cumulative magnetic field was assumed to be 5° . Furthermore, since the resolution of the compass was found to be 5° , an additional uncertainty of 2.5° was assumed.

Since the car was oriented qualitatively relative to the compass by finding a midpoint of the car "by eye" an additional uncertainty of 3° had to be assumed considering the variation of the chosen midpoint during different trials.

The next angular uncertainty that had to be considered is the one stemming from the angular alignment of the box inside of the car. The compass could not be used inside of the car due to interference of magnetic fields, therefore, as explained in Section 2.4, the axis of symmetry of the box was aligned with the axis of symmetry of the car. Due to the qualitative nature of that procedure an error of 2° was assumed.

The final source of angular uncertainty stemmed from rotating the box with detectors relative to the initial placement. Considering that it was performed using a phone compass with 1° angular separation, half of that marking was assumed as the uncertainty.

Considering all the aforementioned sources of angular uncertainty, the total angular uncertainty summed up to 13° .

To improve the setup, a gyroscopic compass, which does not react to external magnetic fields could be used in the future. It would limit the uncertainty stemming from alignment of the car as the compass could be placed directly inside of it. Furthermore, the procedure for aligning both the car and the device inside the car should be improved to be more quantitative rather than qualitative.



4.1.2 Detector Holder Construction Inaccuracies

The support base for mounting the detectors was constructed as precisely as possible; however, due to the materials used and limitations in time and resources, the base presented some minor inaccuracies. These inaccuracies introduced an uncertainty error in the measurements taken. The detector holder base was made of wood, a material that may not maintain a fixed shape and cannot be cut with high precision. The elevation of both holder arms was measured to be 45.0° and 45.3° using a digital spirit level with 0.1° accuracy. The uncertainty of elevation angle was therefore assumed to be 0.4° .

Additionally, the design did not accommodate variations in the terrain where the base was placed. This caused the detector angles to deviate from the intended 45 degrees depending on the setup location, such as on a car or in a park. Manual adjustments using a smartphone level application were necessary, further increasing the measurement error margin.

Another limitation of this setup was the parallel placement of the two pairs of detectors. The mounting method did not ensure that both pairs were exactly 180° apart, as they were secured with screws. This method did not completely fix the base, allowing for some movement and introducing additional uncertainty.

4.1.3 Lacking SD Card Readers in Master Devices

Due to time limitations, it was not possible to order additional SD card readers. This resulted in only the slave devices having the SD card reader module installed. Considering that, it was impossible to determine what was the behaviour of the master devices, as the data of muon detections could only be saved by the slave devices. This meant that the pair was essentially working as a black box without the ability to confirm what its constituent components were registering separately.

In order to improve the calibration of the muon detector in the future, each unit should have an SD card reader module installed. That could help with determining faulty devices and could better explain the relative differences between the number of muon detections of different device pairs.

4.1.4 Cosmic Watch Event Silence and Sensitivities

There were inconsistencies found in the behaviour of the watches after multiple hours of detection. Data gathered from June 24th onwards showed a tendency for the Cosmic Watches to

stop observing muon events after early morning. Furthermore, a test run of the detector at the Stadspark in downtown Maastricht carried out on the 26th from 11:00 to 18:00 showed few to no events during this time. This behaviour may indicate the Cosmic Watches' sensitivity to sunlight and overall radiation may have increased near the end of the experiment. The experiment, carried out June 21st-26th, saw the last daytime measurements taken from 10:00 to 17:00 of the 24th. This day, high temperatures and intense sun heat prompted automatic shut-downs from the Cosmic Watches, as internal temperatures exceeded 40°C. All measurements carried through thereafter were done so from 19:00 to 11:00, during nighttime and early morning, when the aforementioned muon-event silence was also observed near sunrise.

With very little time left in the project, it was not possible to ascertain the source for the change in the nature and sensitivity of the Watches. Although night measurements didn't show much difference from previous ones, the newfound daylight sensitivity could still be due to changes in the scintillators, or their wrapping material. Openings, creases or opacity changes to the aluminum foil and electrical tape under extended exposure to heat may allow for higher quantities of the sunlight and infrared radiation to penetrate into the scintillator. Otherwise, the scintillator's own sensitivity to Gamma radiation may be the source for the overwhelmed, event-silent Watches.

Future experimentation with Cosmic Watches should consider the possible effects of Watch exposure to relatively extreme weather conditions. It is concluded that they should not be exposed to temperatures above 30°C for long periods of time, and that direct exposure to sunlight under these temperatures should be avoided. Furthermore, any future experiments carried out with the specific Cosmic Watches used in this experiment should also consider a lengthy and careful analysis of the scintillators' and Watches' sensitivities, with the idea of possibly changing or re-building components of the SiPM PCB and scintillator complex.

4.2 A Subtle Phenomenon

It was considered after experimentation, and with the reference of external literature and works, that the East-West flux asymmetry is expected to be of the order of a few percent (less than 3 % at $\sim 50^\circ$ of latitude [20]), a precision impossible with the used experimental method. As previously discussed in Section 3.2.1, this precision could only be matched if the variance of the implicit sample distribution of the measurement were small enough to allow confidence in the event count's proper representation of the real muon flux. The current errors associated



with the data are about 6 %.

In order to achieve a relative error small enough for the resolution of the asymmetry, the maximum upper bound is set as $\sigma/x = 0.03$, which means: $1/\sqrt{x} = 0.03 \rightarrow x = 1,111$. Again, x stands for muon events in this context. Following the observed trend during this experiment of ~ 200 muon events every 7 hours, roughly 39 hours of measurement are required to reach this level of accuracy in the data. Taking this a step further (since such an error might still be considered large), confirming a statistical error that is half of the expected asymmetry in magnitude (1.5 %), roughly 4,444 counts, or 155.5 hours of measurement are needed.

The data gathered in this experiment can thus only provide the grounds for future exploration of this topic with the Cosmic Watches. It also shows that accurate measurements of this phenomenon may not be done within the time limits given, unless all tools and preparations were done beforehand.

Future experiments may consider only measuring one singular region in the sky instead of covering a wider azimuth range. However, given the light sensitivity of the Watches, the place of measurement must be indoors, in a dark area and with symmetrical or similar Eastern and Western shielding. Otherwise, a change of location to one of higher altitude or lower latitude for the experiment should be considered, as this would increase overall muon flux.

4.3 Unclear Case for Calibration Method

The aim of the calibration process was to avoid that fluctuations of total muon flux in between the distinct measurements would affect the experimental results. This was done by having a separate set of Watches observe the variation of detection rates, calculating for each interval how much these deviated from the mean. Afterwards, the directional data collected by detectors Billy and Bob could be calibrated with these ratios, according to Equation 4. The experimental data could then verify the accuracy of the calibration method.

Similar to the East-West Asymmetry, the number of counts did not suffice for any concrete conclusions. From Figures 8 and 9, it becomes apparent that the calibration process did not significantly improve nor alter the results. Table 4 underlines this observation.

While the calibrated asymmetry values are slightly closer to the expected value of less than 0.03 (see Section 4.2), attributing the improvement to the calibration fails when taking into account the inherent statistical error of the calibration Watches, as visualized in Figure 7.

Generally, a larger dataset is required for any definitive evaluation.

4.4 Comparison to Literature

This study focused on scanning the azimuthal angle with the muon detectors to study the East-West asymmetry in muon flux. This approach involved rotating the detectors horizontally around a fixed vertical axis to measure the flux of muons arriving from different cardinal directions.

A similar experiment has been conducted at the State University of Campinas in Brazil [21]. Although there is a vast difference in latitude compared to the experiment discussed in this paper, it should still be possible to match the general trends of the East-West Asymmetry. The azimuthal dependence of muon flux is described in Figure 10.

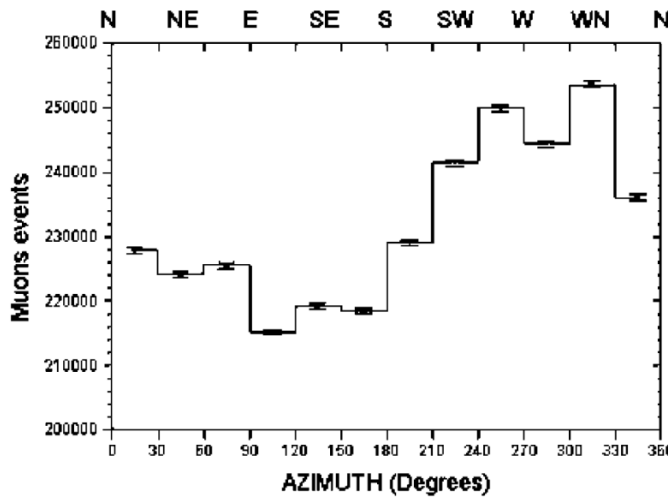


Figure 10: Azimuthal dependence of muon flux as measured in Campinas, Brazil. Data was routinely taken between August 1998 and June 2000, at a zenith angle range of $5^\circ < \vartheta < 45^\circ$. Operation at State University of Campinas, UNICAMP, Brazil [21].

Figure 10 generally agrees with the theory discussed in Section 1.5, with the muon events increasing from East to West. On the other hand, the experiment performed in this paper portrays a different image. Figure 8 seems more unstable, while Figure 9 indicates an opposite asymmetry. Considering the length of data collection and the inherent error coming along with it, as discussed in Section 4.2, one could argue that a longer run would lead to similar conclusions.

There is significant potential for improving the experimental setup described in this paper. A more sophisticated approach, as demonstrated by Pethuraj et al. [22], utilized a 12-layer stack of Resistive Plate Chambers (RPCs) to measure azimuthal dependent muon flux. This indicates that the premise of the experiment, based on the use of CosmicWatch muon detectors, might have already hindered the results.

5 Conclusion

This Cosmic Watch project has demonstrated the extent of the ability to detect cosmic ray muons with an inexpensive detector built by students. The considerable amount of measurements of the flux of these particles could provide valuable insight about cosmic rays and their interactions with environmental factors on their trajectory down to Earth.

The main goal of this project was to study the east-west asymmetry arising in the muon flux. The asymmetries that were found in the experiment disagreed, with one detector pair finding it to be 0.13 and the other -0.04. Thus, the presence of the East-West asymmetry could statistically not be confirmed. This can however serve as reference for further improved research about the geomagnetic impact on the trajectory of cosmic rays. Notably, it was discussed that the time scale of the measurements should be significantly increased for the data to be statistically robust.

A few limitations were encountered during this project, leaving room for future improvement as mentioned throughout this study. The calibration itself did not seem to enhance the results as initially expected. However, it did point out the flaws so as to better the technique and apply it for more precision in future studies.

Overall, this project points out the importance of precise measurements and calibration, robust experimental setup, and thorough data analysis in the context of these studies. Reflecting about the observed limitations, future studies can be built upon this research using it as a reference for future improvement. This will serve as input to the broader understanding of high-energy particles and cosmic phenomena as well as the influence of the trajectory of cosmic rays and their asymmetry across the celestial sphere.

References

- [1] B. Rossi, *Cosmic Rays*. Massachusetts, United States of America: McGraw-Hill, 1964, ISBN: 978-0070538900.
- [2] L. I. Dorman and I. V. Dorman, *Cosmic ray history*. Hauppauge, NY: Nova Science, Dec. 2014.
- [3] CERN contributors, *Anderson and Neddermeyer Discover the Muon*, [Online; accessed 24-June-2024], 2024. [Online]. Available: <https://timeline.web.cern.ch/anderson-and-neddermeyer-discover-muon>.
- [4] M. Tanabashi, K. Hagiwara, K. Hikasa *et al.*, ‘Review of particle physics’, en, *Phys. Rev. D.*, vol. 98, no. 3, Aug. 2018.
- [5] D. Murty, ‘East-west asymmetry of cosmic rays’, *Proc. Indian Acad. Sci.*, vol. 37, pp. 317–320, Aug. 1953.
- [6] S. N. Axani, *The physics behind the cosmicwatch desktop muon detectors*, 2019. arXiv: 1908.00146 [physics.ins-det]. [Online]. Available: <https://arxiv.org/abs/1908.00146>.
- [7] R. A. Mewaldt, ‘Cosmic rays’, *Macmillan Encyclopedia of Physics*, 1996.
- [8] A. R. Bell, ‘Cosmic ray acceleration’, en, *Astropart. Phys.*, vol. 43, pp. 56–70, Mar. 2013.
- [9] L. Lerner, Dec. 2023. [Online]. Available: <https://news.uchicago.edu/explainer/what-are-cosmic-rays#:~:text=Scientists%20believe%20cosmic%20rays%20get>.
- [10] D. Horrocks, *Applications of Liquid Scintillation Counting*. Elsevier, Dec. 2012, ISBN: 9780323154130.
- [11] C. Xu, ‘Study of the silicon photomultipliers and their applications in positron emission tomography’, Jun. 2014.
- [12] V. Rajora and F. Nova, ‘Simulation of cosmic rays in the presence of a magnetic field’, *J Emerg Invest*, 2023.
- [13] H. E. J. Koskinen and E. K. J. Kilpua, *Physics of earth’s radiation belts* (Astronomy and astrophysics library), en, 1st ed. Cham, Switzerland: Springer Nature, Oct. 2021.

- [14] D. S. R. Murty, ‘East-west asymmetry of cosmic rays’, en, *Proc. Indian Acad. Sci. (Math. Sci.)*, vol. 37, no. 2, pp. 317–320, Feb. 1953.
- [15] W. C. Barber, ‘East-west asymmetry and latitude effect of cosmic rays at altitudes up to 33,000 feet’, *Phys. Rev.*, vol. 75, no. 4, pp. 590–599, Feb. 1949.
- [16] U. R. Rao and V. Sarabhai, ‘Time variations of directional cosmic ray intensity at low latitude - II. time variations of east-west asymmetry’, en, *Proc. R. Soc. Lond.*, vol. 263, no. 1312, pp. 118–126, Aug. 1961.
- [17] M. Fukugita and T. Yanagida, *Physics of neutrinos* (Theoretical and Mathematical Physics), en. Berlin, Germany: Springer, Dec. 2010.
- [18] S. N. Axani, K. Frankiewicz and J. M. Conrad, *CosmicWatch: The Desktop Muon Detector Instruction Manual*. 2018. [Online]. Available: <https://www.seti.net/cosmic-rays/SETIPixel/CosmicWatch-Desktop-Muon-Detector-v2-master/Instructions.pdf>.
- [19] G. Knoll, *Radiation Detection and Measurement (4th ed.)* New Jersey, United States of America: John Wiley, 2010, pp. 74–85, ISBN: 978-0-470-13148-0.
- [20] A. Corlin, ‘Cosmic Ultra-Radiation in Northern Sweden’, *Annals of the Observatory of Lund*, vol. 4, A27–A28, Jan. 1934.
- [21] A. C. Fauth and S. Paganini, ‘The east-west asymmetry of single muons at campinas’, *Il Nuovo Cimento C*, 2004. [Online]. Available: <https://api.semanticscholar.org/CorpusID:116301969>.
- [22] S. Pethuraj, G. Majumder, M. Datar, N. Mondal, K. Ravindran and S. Bheesette, ‘Measurement of azimuthal dependent muon flux by 2 m × 2 m rpc stack at iichep-madurai’, *Experimental Astronomy*, vol. 49, Jun. 2020. doi: [10.1007/s10686-020-09655-y](https://doi.org/10.1007/s10686-020-09655-y).

6 Appendix

6.1 Referenced Figures

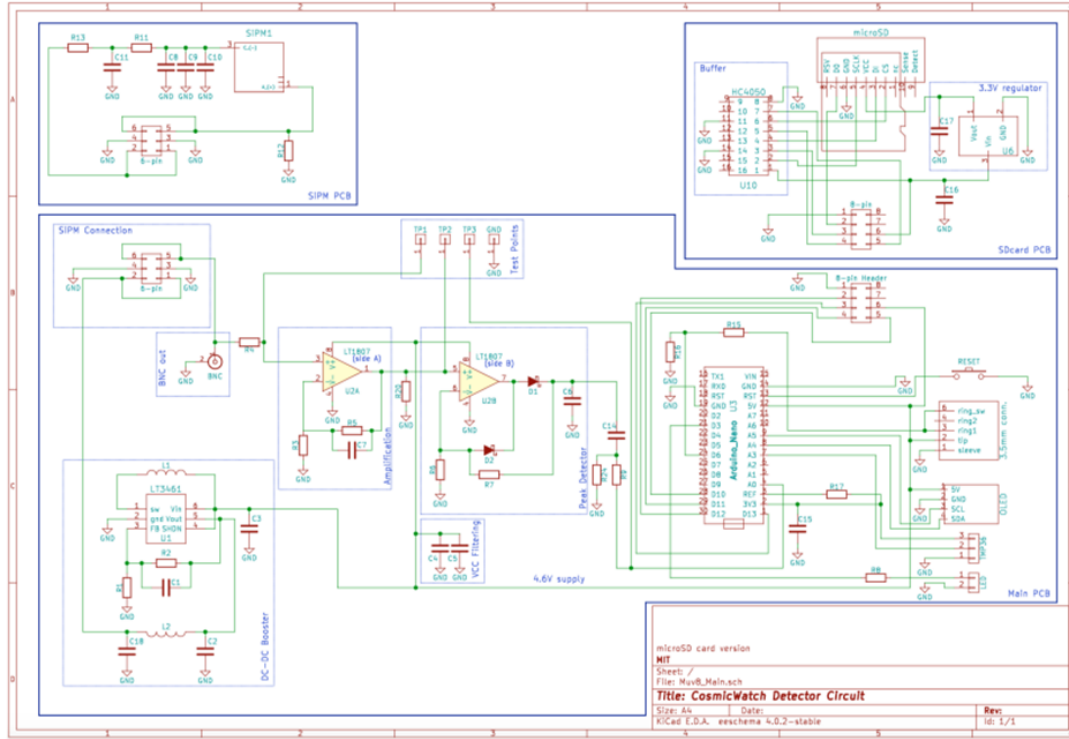


Figure 11: Cosmic Watch Circuit Diagram

6.2 Contributions

6.2.1 Experiment

Pedro Afonso	Background Research
Emre Berna	Soldering, Assembling Detector Support Structure, Experimental Setup and Data Collection, Night Owl
Laura Brijan	Detector Pair Calibration, Location Scouting, Project's Chauffeur, Experimental Setup and Data Collection
Karsten Dekkers	Detector Pair Calibration, Location Scouting, Experimental Setup
Tom Kores Lesjak	Background Research
Miguel Miralda Porrero	Designing Detector Support Structure, Coding of the Calibration and Focused Coverage Area Figure Design
Mathias Perazo	Soldering, PCB Testing, Experimental Setup and Data Collection
Grzegorz Ratajski	Soldering, PCB Testing, Assembling Detector Support Structure, Experimental Setup
Enrique Sanchez	Designing and Assembling Detector Support Structure
Nils Thiessen	Experimental Setup, Coding and Graphing, Detection Pair Calibration, Assembling Detector Support Structure
Indra Vezbergaite	Polishing and Assembling of the Scintillators, Assembling Detector Boxes

6.2.2 Paper

Pedro Afonso	Sections 2.1, 2.2, and 3, Paper Amendments, Proofreading
Emre Berna	Section 2.4, Paper Amendments, Proofreading
Laura Brijan	Section 2.4, Paper Amendments, Proofreading
Karsten Dekkers	Section 4.1.1, Paper Amendments, Proofreading
Tom Kores Lesjak	Sections 1.1, 1.3, 4.2, Paper Amendments, Proofreading
Miguel Miralda Porrero	Sections 1.2, 1.4, 2.3, 3.1.2, Paper Amendments, Proofreading
Mathias Perazo	Sections 3.2.1, 4.1.4, 4.3, Paper Amendments, Proofreading
Grzegorz Ratajski	Sections 4.1.1, 4.1.2, 4.1.3, Paper Amendments, Proofreading
Enrique Sanchez	Section 4.1.3
Nils Thiessen	Sections 1.1, 1.5, 2.3, 3.1, 4.4, Paper Amendments, Proofreading
Indra Vezbergaite	Section 1.1, Conclusion, Paper Amendments, Proofreading